

Molecular Dynamics Simulation of Hydrochloric Acid Ionization at the Surface of Stratospheric Ice

Bradley J. Gertner and James T. Hynes*

Molecular dynamics simulations were used to study the acid ionization of hydrochloric acid (HCl) at the basal plane surface of ice at 190 kelvin, as a model for the acid ionization process in Antarctic polar stratospheric clouds (PSCs). Initial conditions for HCl placement within the top bilayer of the ice lattice were selected on the basis of relevant dynamic equilibrium adsorption-desorption conditions. Free energy changes calculated for the first step in the stepwise acid ionization mechanism ranged from -5.8 to -6.7 kilocalories per mole for various likely initial conditions. These results indicate that acid ionization is thermodynamically favorable and that this process has important implications for ozone depletion mechanisms involving PSCs.

The mechanism of catalytic gas-phase O_3 depletion (1) during the Antarctic spring requires the heterogeneous formation of active chlorine species such as Cl_2 on PSCs from inert chlorine reservoir species such as HCl and $ClONO_2$ (1-7). For these reservoir species to react readily, they must be in ample supply at or near the surface of the PSCs (3). Two primary types of PSCs exist (4) in the Antarctic stratosphere: type I, believed to be primarily nitric acid trihydrate (NAT), and type II, primarily ordinary ice. It is known that HCl is involved in the reactions of many of the other reservoir species (1-7). Here, we focus on the surface HCl acid ionization $ClH + OH_2 \rightarrow Cl^- + HOH_2^+$ on type II PSCs and on the possible ionic character of those reactions (5, 8). Recent experiments have suggested that HCl uptake on ice is limited to approximately the equivalent of one monolayer surface coverage (7, 9, 10), because HCl is not highly soluble in bulk ice (7, 9, 10), and that reaction probabilities and HCl concentrations are greater at the ice surface than on NAT crystals (3). We propose a mechanism, arising from the dynamic character of the ice surface under stratospheric conditions (11), whereby HCl is incorporated into the ice lattice; this process is similar to the matrix encapsulation of $ClONO_2$ suggested by George and co-workers (11); we assume that HCl does not diffuse into the bulk. Using molecular dynamics simulations (12, 13) of HCl on PSC ice at 190 K, we investigated (i) whether the HCl remains molecular or ionizes when so incorporated, (ii) the free energies of the HCl ionization reaction, and (iii) the extent to which liquefaction of the surface plays a role in the (possible) ionization. Our results suggest that the acid ionization process at the ice surface is thermodynamically quite favorable and that the formation of a

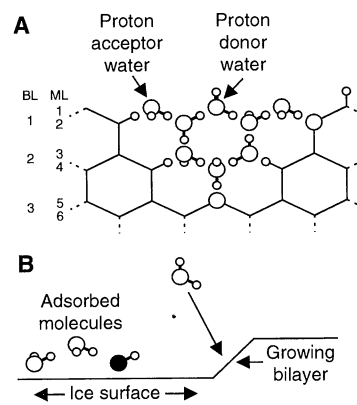
quasi-liquid surface layer (5) is not required to induce ionization.

Hanson and Ravishankara (7) observed that HCl uptake at an ice surface was limited to about a monolayer under stratospherically relevant conditions, and diffusion into the bulk was ruled out. Upon reexposure to HCl after a 5- to 30-min cessation, the HCl uptake was limited to about 40% of that of the unexposed surface, indicating that not all the HCl desorbed when the substrate was no longer exposed to HCl. We interpret these observations as indicators of two forms of HCl at the surface of ice: the readily desorbed HCl ($\sim 40\%$) is weakly adsorbed onto the surface; the remainder ($\sim 60\%$) is incorporated into the lattice but not the bulk.

Fig. 1. (A) Schematic side view of the ice lattice. Rings within each bilayer resemble chair cyclohexane molecules, with alternating molecules comprising one monolayer; the overall ice structure is hexagonal, with the oxygens occupying centers of the tetrahedra. The monolayer (ML) and bilayer (BL) structures are indicated, with lower numbers closer to the ice surface. Each molecule in ML 1 has three hydrogen bonds, and each in the remaining monolayers has four. The triply hydrogen bonded ML 1 waters act either as proton donors or as acceptors, with equal probability (23). In proton acceptor waters, both protons point downward toward nearest neighbor oxygens in ML 2; in donor waters, one proton points straight up. **(B)** Depiction of our view of local ice surface growth one bilayer at a time, where adsorbed HCl and H_2O molecules would be incorporated into the growing bilayer. [Because of the poor solvation of the adsorbed state, we do not expect that the HCl molecule atop the surface is sufficiently solvated to induce ionization (16), making lattice incorporation necessary for possible ionization.] Alternately, if the surface were locally decreasing in size, the adsorbed molecules would desorb along with the surface. Although the time scale for the growth of the bilayer is very large [>1 ms per bilayer (17)] compared to the HCl desorption time theoretically estimated at 130 ns (14), the latter estimate involves only one hydrogen bond and does not allow for the possibility of HCl hydrogen bonding to any adsorbed molecules. The large condensation coefficients and desorption energies of H_2O on crystalline ice measured by George and co-workers (11) suggest that a majority of H_2O molecules are doubly hydrogen-bonded to the ice surface. We propose that most adsorbed waters form short chains of molecules on the ice surface, producing energetically feasible (32) five- and six-membered rings with the surface. These bridges from one surface lattice site to another would increase desorption energies, and thereby increase residence times, of all the adsorbed molecules involved in the chain. We expect that an adsorbed HCl molecule would also rapidly become coupled to a short water chain; a second (even weak) hydrogen bond would increase the HCl residence time sufficiently to make lattice incorporation competitive with desorption (33).

It is not currently known how HCl is incorporated into the ice lattice, how the ice lattice responds to the presence of HCl, or whether HCl ionizes; as a result, there is a lack of knowledge of the likely mechanisms (for example, ionic or molecular) of HCl reactions. In the first computational study of HCl adsorption on PSC ice (14), it was assumed that HCl neither is incorporated into the ice lattice nor ionizes; the resulting calculated surface coverages were orders of magnitude too small as compared with experimental results (7, 9, 10). Although there is some indirect experimental evidence that ionization may occur (7, 9, 15), there is no direct experimental evidence for ionization. One phenomenological model assumes ionization (6), assisted by a proposed quasi-liquid layer (5).

In earlier theoretical work on HCl acid ionization in liquid water, Ando and Hynes (16) found a stepwise proton-transfer mechanism: a first proton transfer from the HCl to a first H_2O , producing the contact ion pair (CIP), and a subsequent proton transfer from the first H_2O to a second H_2O , producing the solvent-separated ion pair. Because the aqueous reaction mechanism (16) showed a dominant, thermodynamically favorable first step to produce the CIP, we used only the first step as our model (17, 18). In the calculation of the HCl acid ionization free energy difference, ΔG , between the molecular pair (MP) state and the CIP state, we used a stepwise implementation of the optimized acceptance ratio



Department of Chemistry and Biochemistry, University of Colorado, Boulder, CO 80309, USA.

*To whom correspondence should be addressed.

method (19, 20). The reaction vacuum component is endothermic by 36.3 kcal/mol (21).

The simulated ice surfaces consisted of three dynamic and two rigid bilayers (13, 14), each bilayer containing 24 molecules (22). We obtained the initial conditions for the sample by first generating four independent pure ice lattices, each obeying the Bernal-Fowler rules for naturally occurring ice (23) before solute introduction. An HCl molecule was then introduced, replacing an appropriately oriented and solvated water molecule (to ensure solute proton orientations in agreement with the descriptions of the cases below), and one neighbor water was reoriented to compensate for the HCl's single proton. For the cases investigated here, we used all four lattices for each of the seven required states (20) and we ran them

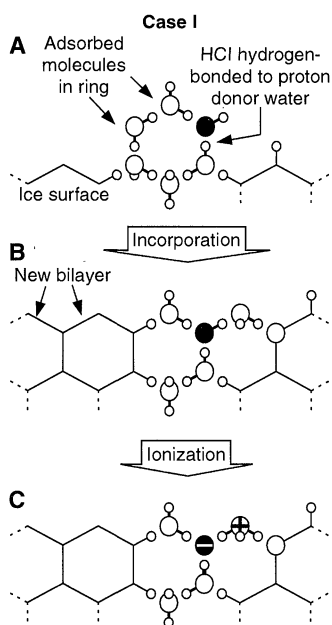


Fig. 2. Depiction of case I. (A) The HCl is hydrogen-bonded to a proton donor water. (B) As the surface layer grows, the adsorbed HCl is incorporated into the second monolayer within the ice lattice, forming the reactant MP. The water depicted acting as a proton acceptor for the HCl (in ML 1) is also a proton acceptor for adsorbing molecules. The chlorine is tetrahedrally coordinated. (C) Placement of the CIP within the lattice: Cl⁻ is in the second monolayer and H₃O⁺ is in the first monolayer. H₃O⁺ prefers three hydrogen bonds (16, 34), leaving only the protons hydrogen-bonded, possible only in the top monolayer, that is, case I; this product solvation is highly favorable. An HCl added to the lower monolayer, with its proton pointing toward the upper monolayer and being hydrogen-bonded to a donor water (not shown), provides tetrahedral solvation of Cl⁻ and trigonal solvation of H₃O⁺; however, the latter has the wrong orientation to benefit from the trigonal solvation. It is unclear if the direct proton transfer would be thermodynamically favorable and it was not investigated here.

for 170 ps, with molecular velocity randomizations at 1-ps intervals. The first 70 ps were used for equilibration (24). The final 100 ps were used in the ΔG calculation (25).

We next focus on the structure and dynamics of the ice surface and how the HCl molecule can be incorporated into the lattice. There are two primary, naturally occurring crystalline ice faces (26), basal plane and prism. Figure 1A depicts the bilayer structure of the stratospherically more relevant basal-plane face of ice, which we chose here (26). George and co-workers (11) demonstrated that ice surfaces are in dynamic equilibrium, continually gaining and losing water molecules. We assume that if the ice surface is locally undergoing growth (Fig. 1B), an HCl molecule adsorbed on the surface is incorporated into the lattice, just as a water molecule would be.

We now discuss the possible reactant positions and orientations within the lattice and their anticipated effects on ΔG . Because the reactant HCl is covalent and only weakly polar (16), its solvation is not particularly sensitive to its lattice placement. But the ionic products will be quite sensitive: Cl⁻ prefers maximum solvation. Because there are a maximum of four nearest

neighbors within the ice lattice structure and there are four nearest neighbors for molecules in the second monolayer or lower, Cl⁻ should prefer to be below the top monolayer. For this study, we did not consider Cl⁻ placement in the top monolayer (27). Because there are only two types of waters with which to hydrogen-bond at the ice surface (see caption of Fig. 1A), an HCl added to the lower monolayer has two possible orientations. If its hydrogen bonding is to a donor water (case I; Fig. 2, A through C), the proton points diagonally upward toward a (future) top monolayer water oxygen (Fig. 2A); because this direct proton transfer has the greatest thermodynamic chance for success (see caption of Fig. 2), we consider this lattice configuration first below. Alternately, if the HCl's hydrogen bonding is to an acceptor water (case II; Fig. 3, A through C), the proton points downward toward the bulk (Fig. 3A). The free energy of the case I acid ionization was $\Delta G = -6.7 \pm 0.9$ kcal/mol (Fig. 4). The reaction is thermodynamically favorable, with only a small barrier of about 2 kcal/mol for the ionization.

To obtain information on the local lattice structure about the MP reactant and the CIP product in case I, at the end of the

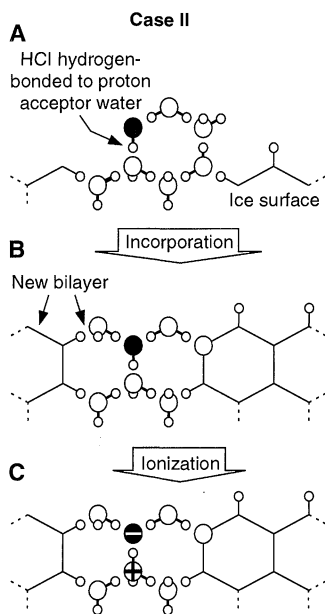


Fig. 3. Depiction of case II. (A) The HCl is hydrogen-bonded to a proton acceptor water. (B) As the surface layer grows, the adsorbed HCl is incorporated into the second monolayer within the ice lattice, as for case I. However, the water acting as a proton acceptor for the HCl is in the third monolayer. (C) Placement of the CIP within the lattice: Cl⁻ is in the second monolayer, and H₃O⁺ is in the third monolayer. One might expect difficulty solvating the products; H₃O⁺ prefers trigonal solvation (see caption of Fig. 2C), whereas the unreorganized lattice provides tetrahedral solvation.

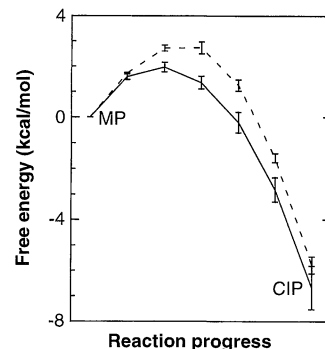


Fig. 4. Free energies of ionization for case I (—) and case II (---). The case I ionization barrier is ≈ 1 kcal/mol lower than the case II barrier, suggesting that details of the solvation mechanism during ionization differ. This difference is also reflected in the overall free energies. The case II H₃O⁺ is well solvated, to the extent that extra charge-dipole complexes (16) are formed (more than four waters solvate the H₃O⁺). This does not occur in case I, where the hydrogen bonds are preferentially determined in the initial conditions. But in case II the charge-dipole complexes compensate for the poor initial solvation conditions for H₃O⁺ production, that is, water that initially hydrogen bonds to the (future) H₃O⁺ oxygen would necessarily reorganize to maximally solvate the cation, in turn causing further solvent reorganization. In the restricted available space, the optimal solution is often cation dipolar solvation (versus hydrogen bonding). Because this all occurs so close to the surface, normal energy penalties for the interaction of H₂O with H₂O evidently do not apply, allowing interactions otherwise forbidden in liquid solution.

trajectories we viewed each of the four reactant state systems and four product state systems in three dimensions and analyzed them for hydrogen bonding. The MP reactant environment varied very little throughout the trajectories: the waters became somewhat more disordered and a few waters left the lattice and were adsorbed atop the lattice, but otherwise the presence of molecular HCl had little effect. Analysis of rotational and translational correlation functions [S_R and S_T , respectively (14, 17)] for the top monolayer ($S_R = 0.16$ and $S_T = 0.22$) indicated some lowering of order relative to that for pure ice (17), but the layer clearly remained solid: for case I, the lattice did not have a liquidlike layer, and yet HCl ionization occurred.

However, the CIP product environment was significantly perturbed. Waters near the Cl^- were strongly hydrogen bonded, and the H_3O^+ tended to bury itself in the lattices. Three of the four systems reorganized such that the H_3O^+ migrated from the first monolayer to the second monolayer; a nearby water moved out of the lattice and atop the H_3O^+ to aid solvation. A value of S_T equal to 0.27 indicated that the CIP system was numerically similar to the molecular HCl system, but the CIP rotational order decreased considerably ($S_R = 0.07$). This suggested a lattice breakdown in the top-most monolayer, although not in the second monolayer ($S_R = 0.30$).

For case II, despite the anticipated poor solvation of the ionic products, ΔG was -5.8 ± 0.3 kcal/mol (Fig. 4), again with only a small barrier, ~ 3 kcal/mol. As in case I, the MP reactant environment changed very little ($S_R = 0.17$, $S_T = 0.33$). Inspected case II CIP systems showed waters near Cl^- strongly hydrogen bonded to it and H_3O^+ well solvated (see caption of Fig. 4). The case II surface could not be considered liquidlike (28).

We have argued that the dynamic character of the ice surface (11) allows the initially molecular HCl to be incorporated into, rather than placed atop, the ice lattice, without incorporation into the bulk. Acid ionization reactions of HCl are thermodynamically favorable, indicating significant HCl ionization at the ice surface (29). Ionic mechanisms (5) are thus important for chlorine activation, and molecular reaction mechanisms involving HCl on PSCs can be eliminated from consideration. The present results strongly suggest that a quasi-liquid layer to induce HCl ionization is unnecessary.

For stronger acids (30) such as HBr and HI under similar conditions, we also expect ionization. At higher temperatures, where vapor pressures must increase to maintain "constant" ice surface thicknesses, more rapid molecular acid lattice incorporation

should accelerate the net ionization. Ionization of strong acids on ice surfaces should have significant implications even for the higher temperature troposphere, where cirrus clouds (mostly ice) provide the condensed medium for reactions (31).

REFERENCES AND NOTES

- S. Solomon, R. R. Garcia, F. S. Rowland, D. J. Wuebbles, *Nature* **321**, 755 (1986); R. J. Cicerone, *Science* **237**, 35 (1987); S. Solomon, *Rev. Geophys.* **26**, 131 (1988); World Meteorological Organization (WMO), *Scientific Assessment of Stratospheric Ozone: 1989* (Rep. No. 20, WMO, Geneva, 1990).
- M. A. Tolbert, M. J. Rossi, R. Malhotra, D. M. Golden, *Science* **238**, 1258 (1987); M. A. Tolbert, M. J. Rossi, D. M. Golden, *ibid.* **240**, 1018 (1988); M.-T. Leu, *Geophys. Res. Lett.* **15**, 17 (1988); *ibid.*, p. 851; M. B. McElroy, R. J. Salawitch, S. C. Wofsy, *Planet. Space Sci.* **36**, 73 (1988); J. M. Rodriguez, M. K. W. Ko, N. D. Sze, *Geophys. Res. Lett.* **15**, 257 (1988); S. C. Wofsy, M. J. Molina, R. J. Salawitch, L. E. Fox, M. B. McElroy, *J. Geophys. Res.* **93**, 2442 (1988); L. T. Chu, M.-T. Leu, L. F. Keyser, *J. Phys. Chem.* **97**, 12798 (1993).
- J. P. D. Abbatt and M. J. Molina, *Geophys. Res. Lett.* **19**, 461 (1992).
- R. P. Turco, O. B. Toon, P. Hamill, *J. Geophys. Res.* **94**, 16493 (1989).
- M. J. Molina, T.-L. Tso, L. T. Molina, F. C.-Y. Wang, *Science* **238**, 1253 (1987).
- A. Tabazadeh and R. P. Turco, *J. Geophys. Res.* **98**, 12727 (1993).
- D. R. Hanson and A. R. Ravishankara, *J. Phys. Chem.* **96**, 2682 (1992).
- J. March, *Advanced Organic Chemistry* (Wiley, New York, ed. 4, 1992); C. M. Nelson and M. Okumura, *J. Phys. Chem.* **96**, 6112 (1992); B.-M. Haas, K. C. Crellin, K. T. Kuwata, M. Okumura, *ibid.* **98**, 6740 (1994); J. M. Van Doren, A. A. Viggiano, R. A. Morris, *J. Am. Chem. Soc.* **116**, 6957 (1994); J. R. Sodeau, A. B. Horn, S. F. Banham, T. G. Koch, *J. Phys. Chem.* **99**, 6258 (1995).
- L. T. Chu, M.-T. Leu, L. F. Keyser, *J. Phys. Chem.* **97**, 7779 (1993).
- J. P. D. Abbatt *et al.*, *J. Geophys. Res.* **97**, 15819 (1992).
- D. R. Haynes, N. J. Tro, S. M. George, *J. Phys. Chem.* **96**, 8502 (1992).
- M. P. Allen and D. J. Tildesley, *Computer Simulation of Liquids* (Clarendon, London, 1987); G. Ciccotti, D. Frenkel, I. R. McDonald, Eds., *Simulation of Liquids and Solids* (North-Holland, New York, 1987); J. Eggbrecht, S. M. Thompson, K. E. Gubbins, *J. Chem. Phys.* **86**, 2299 (1987).
- B. J. Gertner and J. T. Hynes, in preparation.
- G.-J. Kroes and D. C. Clary, *Geophys. Res. Lett.* **19**, 1355 (1992); *J. Phys. Chem.* **96**, 7079 (1992).
- A. B. Horn, M. A. Chesters, M. R. S. McCoustra, J. R. Sodeau, *J. Chem. Soc. Faraday Trans. C*, **88**, 1077 (1992). This experiment was performed at 110 K, where hydrates form, and thus its relevance to the stratosphere is unclear.
- K. Ando and J. T. Hynes, in *Structure and Reactivity in Aqueous Solution: Characterization of Chemical and Biological Systems*, C. J. Cramer and D. G. Truhlar, Eds. (American Chemical Society, Washington, DC, 1994), pp. 143–153; *J. Mol. Liq.* **64**, 25 (1995); in preparation. The ΔG of HCl ionization in liquid water calculated for the CIP is -6.7 kcal/mol, and the overall experimental reaction ΔG is roughly -8 to -10 kcal/mol. With an estimated additional stabilization at infinite separation of less than 1 kcal/mol, the former is a numerically reasonable estimate for the aqueous ionization.
- Comparison of liquid-state water models can be found in W. L. Jorgensen, J. Chandrasekhar, J. D. Madura, R. W. Impey, M. L. Klein, *J. Chem. Phys.* **79**, 926 (1983). For analysis of TIP4P waters, used in the present study, at 190 K, see G.-J. Kroes, *Surface Sci.* **275**, 365 (1992). Calculated rotational and translational correlation function values for pure ice are $S_R = 0.24$ and $S_T = 0.43$, respectively.
- Test simulations with the TIP3P (17) water model used in the liquid-state work (16) did not produce a stable ice surface at 190 K; therefore, we used here the similar but more suitable TIP4P water model with a stable ice surface (17), which required the recalculation of some parameters. We used the previously determined (16) Cl–O separation of 2.96 Å, found to be quite stable to solvent perturbations, for the reactant $\text{ClH} \cdots \text{OH}_2$ MP and the product $\text{Cl}^- \cdots \text{HOH}_2^+$ CIP. We optimized (16) the parameters for the isolated HCl–water interaction and the isolated H_3O^+ –water interaction, using TIP4P waters. The effective chlorine charges in Ando and Hynes (16) for the MP and CIP states were -0.417 and -0.846 , respectively. The charge localized on the oxygen in the CIP state represents approximately three-quarters of the total possible charge shift from the MP state to the fully ionic state. This charge shift was implemented here as a linear combination of molecular and ionic states, with effective chlorine charges of -0.364 and -0.841 , respectively, for the MP and CIP states, derived from the molecular HCl interactions with TIP4P waters. The H_2O – H_3O^+ charges were similarly defined; in the CIP state the atomic charges were one-quarter those of H_2O and three-quarters those of the fully ionic H_3O^+ .
- C. H. Bennett, *J. Comput. Phys.* **22**, 245 (1976). This method minimizes the variance of the finite-sample free energy estimate $\Delta G_{1,0}$ of a two-state free energy calculation by sampling the potential energy difference between states, $\Delta E_{1,0} = V_1 - V_0$, from both states, for example, the reactant and product states.
- We implemented the method (19) stepwise, so that the ΔE distributions from each state had significant overlap (the large sample regime). This required five intermediate states between reactants and products (seven total), each state generated as a linear combination of the molecular and ionic states. The resultant ΔG estimate is the sum of the intermediate estimates (19). The sequence of (fixed) intermediate states with equilibrated solvent closely resembles an equilibrium solvation reaction path in ΔE [see (16) and J. Juanós i Timoneda and J. T. Hynes, *J. Phys. Chem.* **95**, 10431 (1991)].
- The free energy vacuum component was calculated as follows. Using the GAMESS electronic structure system [M. W. Schmidt *et al.*, *J. Comput. Chem.* **14**, 1347 (1993)], we calculated the vacuum ionization endothermicity of the HCl– H_2O dimer as 34.7 kcal/mol. Using the data in (16), we estimated the zero-point energy change at a CIP destabilization of 1.6 kcal/mol. The net correction was 36.3 kcal/mol. The five intermediate-state energies were linearly interpolated between those of the MP and CIP states.
- Rigid body rotational molecular motions were implemented with quaternions (12) in a Hamiltonian representation (13). The Verlet algorithm (12) was used to integrate Hamilton's equations (6.25-fs time step). Because the system is anisotropic, special semi-infinite periodic boundary conditions have been developed (13) to handle the long-range Coulombic interactions: (i) an accelerated two-dimensional Ewald sum technique that eliminates convergence problems [J. Hautman and M. L. Klein, *Mol. Phys.* **75**, 379 (1992)]; (ii) a dielectric continuum representation of the bulk ice lying below the sample but not explicitly evaluated in the simulation; and (iii) a hexagonal box to minimize cubic boundary condition artifacts and to maximize solute-solvent interaction efficiency. The boundary conditions allowed system size reduction without significant truncation errors or convergence problems. The periodic image of the HCl molecule is approximately 15 Å from the original HCl. For the CIP, there will be significant image screening in the ice that has a high dielectric constant. Because the simulations were used only for equilibrium properties, all protons were replaced by deuterons to improve numerical accuracy and computational efficiency.
- J. D. Bernal and R. H. Fowler, *J. Chem. Phys.* **1**, 515 (1933).
- To reduce the effects of spurious, large interaction forces due to solute insertion, we integrated the first picosecond, using the following scheme. For the first

Structure and Evolution of Lithospheric Slab Beneath the Sunda Arc, Indonesia

Sri Widiyantoro* and Rob van der Hilst†

Tomographic imaging reveals seismic anomalies beneath the Sunda island arc, Indonesia, that suggest that the lithospheric slab penetrates to a depth of at least 1500 kilometers. The Sunda slab forms the eastern end of a deep anomaly associated with the past subduction of the plate underlying the Mesozoic Tethys Ocean. In accord with previous studies, the lithospheric slab was imaged as a continuous feature from the surface to the lower mantle below Java, with a local deflection where the slab continues into the lower mantle. The deep slab seems to be detached from the upper mantle slab beneath Sumatra. This complex slab structure is related to the Tertiary evolution of southeastern Asia and the Indian Ocean region.

The tectonic evolution of island arcs and lithospheric fragments in southeastern Asia is complex because of the interaction of several lithospheric plates (Fig. 1A) (1–3). Without sufficient land-based paleomagnetic measurements and information about the structure of the deep Earth, the relative plate motion in this complex plate boundary zone has often been reconstructed from data on ocean-floor spreading of the major oceanic plates using geometrical fits on a sphere (4). Seismic imaging provides information about Earth's interior structure that helps understanding of the geological history. Here, we focus on the northward subduction of the complex Indo-Australian Plate along the Sunda arc (from northwestern Sumatra, along Java, to Flores).

In the east, continental lithosphere (Australia) has been colliding with the Banda arc since about 5 million years ago (Ma), whereas further to the west, the oceanic part of the Indo-Australian Plate subducts beneath the Java trench. The age of the subducting ocean floor varies from 50 to 90 Ma along Sumatra to 100 to 135 Ma and 140 to 160 Ma near Java and Flores, respectively. The lateral variation of the nature and age of the subducting plate influences the style of deformation and seismicity along the Sunda arc (5). Earthquakes with focal depths of up to 670 km occur in the steeply dipping (~60°) seismic zone beneath the Java arc, but there is a seismic gap between depths of 350 and 500 km (6–8). Beneath Sumatra, the seismic zone dips ~30° to 45°, but there are no earthquakes deeper than 300 km, which has been attributed to the relatively young age of subducted lithosphere (8, 9).

We inferred from the tomographic im-

ages that the slab is continuous across the seismic gap beneath Java and that there is a pronounced seismic anomaly in the lower mantle. This is in good agreement with conclusions based on previous tomographic studies (10, 11), even though different data sets and reference Earth models were used, leaving little doubt that the deep Java slab is a realistic structural feature. In addition, we (i) present evidence for a lower mantle anomaly beneath Sumatra and for the detachment of the upper mantle slab from the deeper slab, (ii) explore the substantial lateral variation in slab morphology, and (iii) discuss the geological evolution of the lithospheric slab, which seems to be more complex than that of the western Pacific subduction zones (12, 13).

We investigated mantle structure beneath the Indonesian region (Fig. 1A) by means of tomographic images produced by linearized inversion of travel-time data of direct *P* phases and the surface-reflected depth phases *pP* and *pwP* (14, 15). The radially stratified *iasp91* model (16) was used as a global reference for the seismic velocities and for the tracing of the ray paths. The inclusion of the depth phases improved the sampling of mantle structure away from the seismic zones, in particular beneath the back arc regions (Fig. 1, A and B), and provided constraints on earthquake focal depth. The hypocenters and phase data used were derived from the reprocessing of the entire data catalog of the International Seismological Centre, which involved nonlinear hypocenter relocation and phase reidentification (17). This data set was augmented by data from the Australian *Skippy* project (18). We used about 1.3 million data, constituting a linear system of about 275,000 equations (19), from nearly 17,000 earthquakes within the study area recorded at one or more of over 2000 seismological stations worldwide. Following Fukao *et al.* (10), we inverted both regional and global structure simultaneously to minimize contamination of our regional model

Research School of Earth Sciences, Australian National University, Canberra, ACT 0200, Australia.

*On leave from the Department of Geophysics, Bandung Institute of Technology, Bandung 40132, Indonesia.

†Present address: Department of Earth, Atmospheric, and Planetary Sciences, Massachusetts Institute of Technology, Cambridge, MA 02139, USA.

50 fs, the integration step was set at 1.25 fs, and the momenta were randomized every 5 fs. For the next 150 fs, they were set at 2.5 fs and 10 fs. For the remaining 800 fs we used an integration step of 5 fs, with randomizations every 10 fs.

25. We ran 28 trajectories per case, representing a total simulation time of 9.52 ns, using 290 central processing unit (CPU) hours on an IBM/RS6000 model 590 computer (5.6 ns) and another 650 CPU hours on an Apple Power Macintosh 7100/82 computer (3.92 ns). Increasing equilibration times above 70 ps (and thus decreasing data collection times below 100 ps) showed no significant difference.
26. S. C. Colbeck, *J. Cryst. Growth* **72**, 726 (1985). Although temperatures above 253 K were dealt with, no change in behavior below 263 K was reported. The relative surface area of the basal-plane faces was somewhat greater than that of the prism faces below 263 K. Thus, the basal-plane face is expected to be more relevant at 190 K.
27. The thermodynamics of the various configurations have not been investigated. We addressed here only HCl additions to the second bilayer, which we believe are likely made during the barrierless adsorption process. Stable additions to the uppermost bilayer are also possible, as part of bilayer formation or as a result of the replacement of existing waters; however, we believe both of these are activated processes and thus did not consider upper monolayer sites in this first investigation.
28. There were numerically observable second-bilayer effects. For case II, $S_R = 0.70$ and $S_T = 0.70$ for the molecular reactants in monolayer 3, but $S_R = 0.60$ and $S_T = 0.57$ for the CIP products. By contrast, there was no significant change for case I; $S_R = 0.68$ and $S_T = 0.68$ for the molecular reactants in monolayer 3, and $S_R = 0.68$ and $S_T = 0.69$ for the CIP products.
29. We inferred above from experiment (7) that these sites represent the majority of HCl available for reaction on the basal-plane face. For completeness, the remaining HCl atop the surface will need to be examined in the future (along with the prism face and surface defects). After this work was completed, we became aware of the work of S. H. Robertson and D. C. Clary, *Faraday Discuss. Chem. Soc.*, in press. The authors suggest that HCl ionization is energetically favorable from the adsorption site atop the ice surface identified in (14). However, these calculations did not establish that the free energy of the CIP in its equilibrated ice surroundings is lower than the corresponding quantity for the MP.
30. D. R. Hanson and A. R. Ravishankara, *J. Phys. Chem.* **96**, 9441 (1992).
31. L. A. Barrie, in *The Tropospheric Chemistry of Ozone in the Polar Regions*, H. Niki and K. H. Becker, Eds. (Springer-Verlag, New York, 1993), pp. 3–24.
32. R. N. Pribble and T. S. Zwier, *Science* **265**, 75 (1994).
33. If the HCl–H₂O hydrogen bond strength of (14) is doubled (from 4.7 to 9.4 kcal/mol) to account for two hydrogen bonds, the residence time increases to ~30 ms. An alternative estimate of a residence time is ~0.8 ms, based on the experimentally estimated 8 kcal/mol desorption energy of (molecularly adsorbed) α -HCl on HCl · (H₂O)₆ at 140 K, reported by J. D. Graham and J. T. Roberts [*J. Phys. Chem.* **98**, 5974 (1994)]. An HCl with two hydrogen bonds would not be expected to ionize [see (16) and M. J. Packer and D. C. Clary, *J. Phys. Chem.* **99**, 14323 (1995)].
34. M. D. Newton, *J. Chem. Phys.* **67**, 5535 (1977).
35. We thank K. Ando for assistance with the electronic structure calculations and gratefully acknowledge useful conversations with R. Bianco, S. M. George, A. R. Ravishankara, J. T. Roberts, M. A. Tolbert, and V. Vaida. This work was supported in part by a grant from the Petroleum Research Fund, administered by the American Chemical Society, by National Science Foundation grant CHE 93-12267, and by a special Scientific Computing Division grant for supercomputer time from the National Center for Atmospheric Research.

8 November 1995; accepted 22 January 1996